ACS Catalysis

Letter

pubs.acs.org/acscatalysis

Mesoporous Silica-Supported Ruthenium Oxide Nanoparticulates as Efficient Catalysts for Photoinduced Water Oxidation

Yang Zhang,[†] Eileen C. Judkins,[†] David R. McMillin,[†] Dhairya Mehta,[‡] and Tong Ren*[,†]

[†]Department of Chemistry and [‡]School of Chemical Engineering, Purdue University, West Lafayette, Indiana 47907, United States

Supporting Information

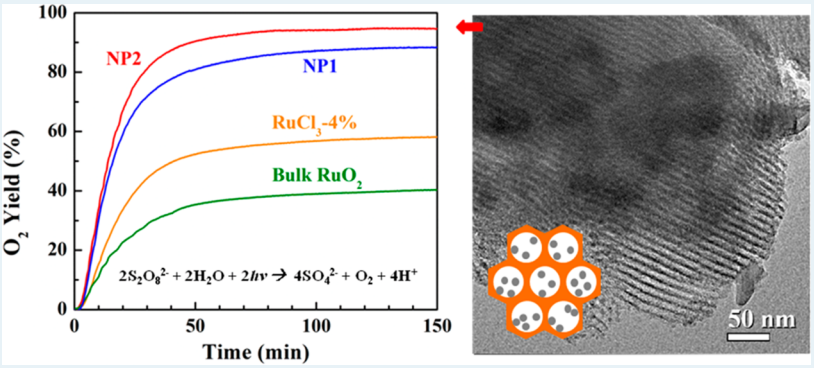

ABSTRACT: The preparation of nanoparticulate RuO_2 supported on mesoporous silica SBA-15 was optimized to achieve a uniform dispersion and confinement of RuO_2. The supported RuO_2 (NP2) has been used as the catalyst for photoinduced water oxidation with $Ru(bpy)_3^{2+}$ as the photosensitizer and $S_2O_8^{2-}$ as the sacrificial oxidant. Both NP2 and the previously prepared NP1 achieved O_2 yields (based on $S_2O_8^{2-}$) of 95% and 88% and overall quantum efficiencies of 11.3% and 10.0%, respectively. These benchmark numbers far exceed those of many other metal oxide-based catalysts and previously reported RuO_2 catalysts. In addition, NP2 has been recycled up to five times with minimal loss of activity.

KEYWORDS: *RuO_2, mesoporous silica, photoinduced water oxidation, catalyst, nanoparticulate*

Hydrogen gas has long been considered an environmentally benign and renewable alternative to carbon fuels.[1] A central thrust in current research on hydrogen generation focuses on photoinduced water splitting.[1,2] The development of viable and efficient catalysts that facilitate O_2 production remains the major challenge in the study of the corresponding half-reaction of water oxidation.[3] A widely used approach for testing photocatalysts involves $Ru(bpy)_3^{2+}$ (bpy = 2,2′-bipyridine) as the photosensitizer and $S_2O_8^{2-}$ as the sacrificial oxidizing agent.[4] The overall net reaction can be expressed as[3]

$$2S_2O_8^{2-} + 2H_2O + 2h\nu \rightarrow 4SO_4^{2-} + O_2 + 4H^+ \quad (1)$$

A plethora of homogeneous catalysts for water oxidation, both electrochemical and photochemical in which the robustness of catalyst is a general concern have been reported and reviewed in recent years.[3,5] In a few recent examples, metal oxide particles derived from molecular precursors were unambiguously identified as the active species,[6] and the poisoning of a Ru-based molecular catalyst by carbon monoxide derived from degraded catalyst was noted, as well.[7] In comparison, heterogeneous catalysts based on metal oxide are advantageous over homogeneous catalysts in their stability, recyclability, and ability to realize the multielectron transfer process in O_2 evolution.

For the development of heterogeneous metal oxide catalysts, minimizing the size of the catalyst and preventing severe aggregation are the keys to obtaining a high turnover number (TON) and improving the photon utilization efficiency and turnover frequency (TOF). To achieve these goals, the utilization of porous support materials has been developed. A number of porous silica-supported, nanosized metal oxides have been reported as active catalysts for H_2O oxidation, including RuO_2,[8] IrO_2,[8,9] Co_3O_4,[10] and Mn_xO_y.[11] These reports demonstrate significant improvement in catalytic activity and stability compared with unsupported or bulk metal oxides. Nonetheless, several important performance benchmarks, such as the nonstoichiometric production of O_2 or low quantum efficiency, remain to be improved.

Owing to its low overpotential,[12] RuO_2 has been known as one of the most active binary metal oxide catalysts for water oxidation since the late 1970s.[13] A series of Y-zeolite-supported RuO_x and RuO_x–IrO_x were reported as the catalysts for photoinduced water oxidation by Lehn in 1980,[8] and a similar series of RuO_2/Y-zeolite-based catalysts was reported by Dutta.[14] These early studies demonstrated both the excellent

Received: July 26, 2013
Revised: September 26, 2013
Published: September 30, 2013

   dx.doi.org/10.1021/cs4006106 | ACS Catal. 2013, 3, 2474–2478

Scheme 1. The Synthetic Procedures for (a) NP1 and (b) NP2

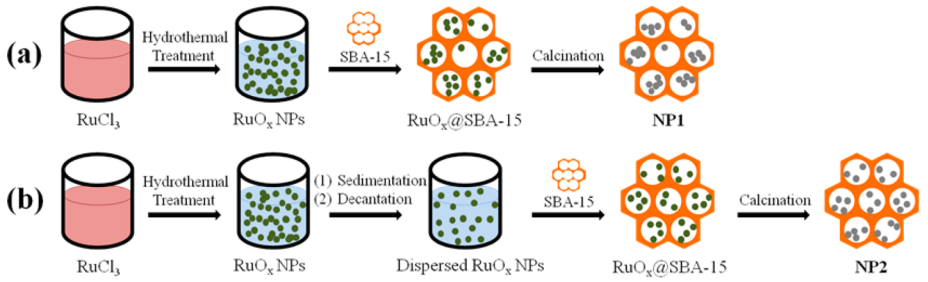

performance of RuO_2 in water oxidation and the role of zeolite supports in enhancing the dispersion and surface area of catalysts.

Mesoporous silica have been widely used as the support of catalysts[15] since the discovery of both the MCM series[16] and the SBA series.[17] Recently, we reported the preparation of nanoparticulate (NP) RuO_2 supported on mesoporous silica SBA-15 (NP1; previously denoted as NP-4%) and its catalytic application for water oxidation using the sacrificial oxidant Ce^{IV}.[18] NP1 was proven quite robust (its TON exceeded 200) and also the most efficient among all RuO_2-based catalysts, including a mesoporous silica-supported RuO_2 catalyst reported by Bruce.[19] The efficiency of NP1 is largely attributed to the high effective surface area of supported RuO_2, which was retained through the confinement effect of the mesoporous host that prevents RuO_2 nanoparticulates from extensive aggregation during both the post treatments and catalytic experiments. Reported herein are (1) further improvement of the NP synthesis to yield NP2 and (2) demonstration of the utility of both NP1 and NP2 in catalyzing photoinduced water oxidation.

The previously reported procedure for the synthesis of NP1[18] is illustrated in Scheme 1a. The presynthesized RuO_x nanoparticulates (~1.6 nm)[20] were dispersed in water and loaded into mesoporous silica SBA-15 at a 4 wt % ratio by stirring and sonication, followed by the removal of water and the immobilization of NPs into SBA-15 by simple calcination. In the present study, an additional step of sedimentation and decantation was introduced to further reduce the aggregation of nanoparticulates (Scheme 1b). After $RuO_2{\cdot}xH_2O$ was redispersed in water, instead of directly mixing with SBA-15, the suspension was kept static without stirring for 1 week. The dispersion retained a dark black color with agglomerated $RuO_2{\cdot}xH_2O$ precipitated at the bottom. After decantation, the fine suspension was mixed with SBA-15 at the same weight percentage of $RuO_2{\cdot}xH_2O$ as for NP1. The concentrations of $RuO_2{\cdot}xH_2O$ in the suspension before and after sedimentation were measured as 3.0 and 0.8 mg/mL, respectively. The remaining steps for immobilization were identical to those of NP1, and the resultant supported RuO_2 was named NP2. The actual loading of RuO_2 is 4.0 ± 0.3 wt %, estimated on the basis of the weight increase from SBA-15 to NP2 as well as the mass of dried precipitate after decantation.

Figure 1a shows a typical TEM image of NP2. The shadowed areas in this image are attributed to RuO_2 nanoparticulates. The shadows are light in grayscale and quite scattered throughout the porous framework, indicating excellent dispersion of RuO_2 within the pores. Furthermore, this image reveals hardly any noticeable dark spots that were observed in the TEM image of NP1,[18] suggesting a low degree of aggregation of RuO_2 in NP2. Figure 1b shows a high-resolution TEM image close to the

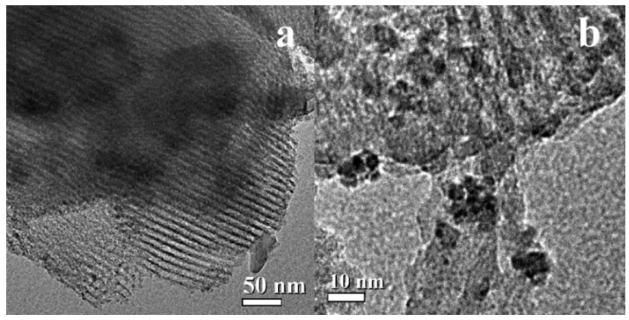

Figure 1. (a, b) TEM images of NP2.

surface of the silica support, where the particles tend to severely agglomerate; however, in this case, the RuO_2 nanoparticles within the mesopores (at the upper side of this image) are adequately separated, and on the disordered silica surface, the spots with sizes around 10 nm consisted of only 3−6 distinguishable particles.

Supported oxygen-evolving catalysts with such small particle sizes are scarce. For instance, both Co_3O_4/SBA-15[10] and MnO_x/KIT-6[11] composites prepared in the laboratory of Frei consist of catalyst particles larger than 50 nm, and Co_3O_4/ KIT-6 reported by Jiao contains particles of ~25 nm diameter.[21] The only supported catalyst with size comparable to the RuO_2 particles was reported by Bruce,[19] for which a very elaborate synthetic path dictated the smallness of the mesopores (<3 nm) and the limited exposure of the catalytic particles that were embedded in the silica walls. These factors possibly restrict the mass transfer within the pores and the contact between the liquid phase and the nanoparticles, leading to slower water oxidation than that of NP1.[18] It is worth mentioning that in Figure 1b, the ordering of the mesopores started deteriorating under the intense electron beam while the nanoparticles stayed intact. Figure S1 in the Supporting Information shows the same area less exposed to the electron beam, where mesoporous ordering was better preserved. The robustness of the dark particles under the intense electron beam is consistent with the fact that these darker sites consist of RuO_2 rather than silica.[19] The above description confirms that the sedimentation procedure effectively removed the majority of the aggregated RuO_2 NPs and resulted in a better-dispersed distribution of NPs within the silica framework than NP1 and that RuO_2 remained as nanoscale particulates without serious fusion during loading and calcination. This conclusion is further supported by the powder X-ray diffraction patterns (Supporting Information Figure S2). Compared with submicrometer-sized RuO_2 supported on SBA-15 (denoted as $RuCl_3$-4%[18]) and commercial bulk anhydrous RuO_2, both of which yielded peaks characteristic of rutile-structured RuO_2, neither NP sample

dx.doi.org/10.1021/cs4006106 | ACS Catal. 2013, 3, 2474−2478

showed distinguishable peaks. This is indicative of the low degree of fusion and crystallization[10,11] of RuO_2 due to the restriction effect of the silica walls on RuO_2 aggregation.

The effect of catalyst loading on the porosity of SBA-15 was analyzed with nitrogen sorption experiments. The BET areas of NP2 and NP1 are 534 and 531 $m^2\ g^{-1}$, and pore volumes obtained at $P/P_0 = 0.99$ are 0.70 and 0.68 $cm^3\ g^{-1}$, respectively. The reduction in both surface areas and pore volumes of the two samples compared with that of the original SBA-15 (575 $m^2\ g^{-1}$ and 0.75 $cm^3\ g^{-1}$) are only 7−9%, indicating the scarcity of mesopore blockages by the loaded catalysts. Figure 2a shows

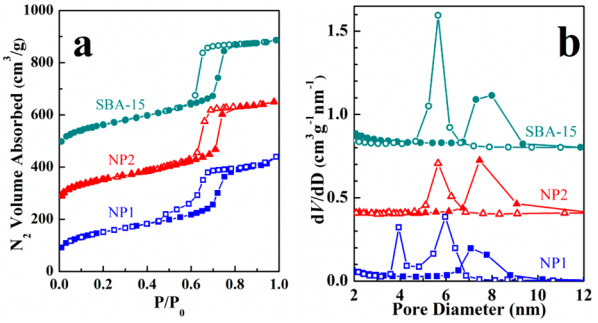

Figure 2. (a) Nitrogen sorption isotherms of SBA-15, NP2, and NP1 and (b) the corresponding pore size distributions (2−12 nm) calculated from adsorption (solid) and desorption (hollow) branches via the Barrett−Joyner−Halenda (BJH) method. The isotherms of NP2 and SBA-15 are offset vertically by 200 and 400 $cm^3\ g^{-1}$, and the pore diameter distributions of NP2 and SBA-15 are shifted by 0.4 and 0.8 $cm^3\ g^{-1}\ nm^{-1}$, respectively.

the isotherms of SBA-15, NP2, and NP1. SBA-15 and NP2 exhibit typical H_1 hysteresis loops. NP1 differs in the desorption branch where the convergence of adsorption and desorption branches is postponed to $P/P_0 \sim 0.45$, in comparison with ∼0.6 for SBA-15 and NP2. The delayed convergence of the two branches often happens to pores possessing a bottleneck-type structure, in which the entrance is smaller than the internal pore.[22] For NP1, the characteristic two-step desorption branch and the delayed convergence therefore indicate that RuO_2 is successfully loaded into the pores, although a fraction of the entering or internal pores are narrowed by the catalyst.[23] The lack of such characteristics in NP2 thus suggests that RuO_2 nanoparticulates are scattered enough that the pore size is not influenced by their loading. The pore size distributions (Figure 2b) also show that all three samples possess the same pore diameter of 7−8 nm (from adsorption branches), but only NP1 has mesopores partially narrowed by the loaded catalyst (indicated by the additional distribution at 3.5−6 nm in the desorption branch).

NP2 and NP1 were tested as catalysts for photoinduced water oxidation. For comparison, reactions were also tested for $RuCl_3$-4% and commercial unsupported bulk RuO_2 under the same conditions. For each reaction, 12 mg of supported catalyst or 0.48 mg of RuO_2 (3.6 μmol of RuO_2, set as 1.0 equiv) was dispersed in a $Na_2SiF_6/NaHCO_3$ buffered solution[10] (pH = 5.4) with 1 equiv of $Ru(bpy)_3Cl_2{\cdot}6H_2O$, 9 equiv of $Na_2S_2O_8$, and 45 equiv of Na_2SO_4. A light source of 454 nm wavelength was used to excite the sensitizer. An Ocean Optics FOSPOR-R oxygen sensor was adapted for real-time monitoring of the evolved oxygen in the headspace. Leaking of the air in the headspace was either negligible (<1% of the yield within 24 h) or calibrated for, and additional light harvesting due to outside light leaking into the reaction system was minimal (<1%).

Figure 3a shows the percentage of oxygen generated based on the stoichiometry of $Na_2S_2O_8$, where 100% yield

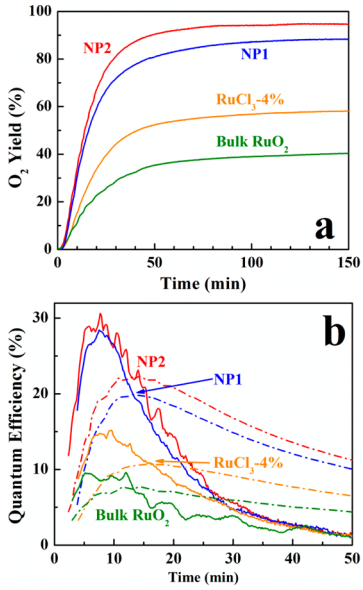

Figure 3. (a) Oxygen gas evolution catalyzed by NP2, NP1, $RuCl_3$-4%, and bulk RuO_2 and (b) instantaneous (solid lines) and cumulative (broken lines) Φ values of corresponding reactions.

corresponds to the complete conversion of $Na_2S_2O_8$ to O_2. The initial TOF of each sample, defined as 4 times (because the oxidation of water is a $4e^-$ process) the rate of the generation of O_2 per RuO_2 unit per minute right after the induction period, was calculated on the basis of the linear fitting of the data between 5 and 15 min (every adjusted R^2 for the fitting is 0.997 or higher), with the induction period of 0−5 min being truncated. The calculated TOFs and the yields of O_2 (at 150 min) are 1.64 min^{-1} and 95% for NP2, 1.48 min^{-1} and 88% for NP1, 0.84 min^{-1} and 61% for $RuCl_3$-4%, and 0.52 min^{-1} and 40% for bulk RuO_2. The NP series, especially NP2, shows excellent performance in achieving both high TOFs and nearly quantitative O_2 yields. The RuO_x/Y-zeolite-catalyzed photo-induced water oxidations were reported by Lehn[8] and Dutta,[14] with TOFs and yields of O_2 of 0.24 min^{-1} and 31% and 0.11 min^{-1} and 30%, respectively. Recently, the Yoshida group reported the incorporation of RuO_2 nanoparticles into polymer gel,[24] which exhibited a TOF and yield of 1.0 min^{-1} and 20%, respectively. Although a direct comparison is hard to make because of the difference in test conditions (temperature, photon influx, concentrations of chemicals and oxidizing agents), it is clear that the NP series enables much higher O_2 yields. It is also noteworthy that the O_2 yield for NP2 is better than those obtained using other metal oxides under similar catalytic conditions, for example, 35−65 nm sized Mn_xO_y nanobundles (55%)[11] and 70−90 nm Co_3O_4 nanoclusters (58%)[10] supported on mesoporous silica; Co ions embedded in porous aluminum phosphate (17%);[25] and unsupported particles of IrO_2 (69%),[26] $LaCoO_3$ (74%),[27] and $NiFe_2O_4$ (74%).[28]

The excellence of NP2 in the catalysis of water oxidation can be attributed to the intrinsically high activity of Ru species toward water oxidation[12] and the smaller size and better

dx.doi.org/10.1021/cs4006106 | ACS Catal. 2013, 3, 2474−2478

dispersion of RuO_2 naoparticulates. It is known that photoexcited $Ru(bpy)_3^{2+*}$ is oxidized by $S_2O_8^{2-}$ to $Ru(bpy)_3^{3+}$, which is subject to degradation due to the nucleophilic attack of water and OH^- before reaching the surface of the catalyst, where the electron transfer from the catalyst to $Ru(bpy)_3^{3+}$ happens.[25,28,29] Hence, the high surface area of RuO_2 in NP2 enables more expedient access of $Ru(bpy)_3^{3+}$ to catalytic sites, which contributes to a high TOF.

Because of the difference in reaction conditions, it is impractical to make a direct comparison of various catalytic systems on the basis of O_2 evolution rate and TOF. To further compound the problem in the comparison of photocatalytic reactions with other literature reports, the photon influxes in different experimental setups are hardly comparable or often not specified in the papers. Hence, a meaningful comparison with literatures should be based on quantum efficiency (Φ). In this report, the photon-influx from the light source to the cuvette was measured via chemical actinometry,[30] and then both the cumulative and instantaneous Φ of the overall reaction system were estimated on the basis of the equations below, where each absorbed photon corresponds to the transfer of two electrons.[31]

$$\text{cumulative } \Phi = \frac{2 \times \text{O}_2 \text{ molecules produced since 0 min}}{\text{photons absorbed by rxn suspension since 0 min}} \times 100\% \quad (2)$$

$$\text{instantaneous } \Phi = \frac{2 \times \text{rate of O}_2 \text{ molecules production at time } t}{\text{rate of photon absorption by rxn suspension at time } t} \times 100\% \quad (3)$$

Figure 3b provides a qualitative trend of Φ: it increases after an induction period, peaks at 8 min (for both NP2 and NP1), 9 min ($RuCl_3$-4%), or 12 min (bulk RuO_2), and then gradually decays. The order of photon utilization efficiency is as follows: NP2 > NP1 > $RuCl_3$-4% > bulk RuO_2. The highest instantaneous Φ for NP2 is 31%, evident of the excellent photon utilization efficiency of NP2 system. Cumulative Φ data similarly prove that the series of RuO_2 catalysts, especially NP2, utilizes the photon energy more efficiently: at 50 min, the cumulative Φ is 11.3%, 10.0%, 6.5%, and 4.4% for NP2, NP1, $RuCl_3$-4%, and bulk RuO_2, respectively. Supported metal oxide IrO_2,[32] Co_3O_4,[10] and Mn_xO_y[11] nanoparticles have reported Φ values of 11%, 18%, and 11%, respectively; however, these reported Φ values were based on the initial rates (the maximal rates) of oxygen evolution, which do not reflect the true cumulative Φ throughout the entire course of reaction. In the present study, the maximal instantaneous Φs (at ∼10 min) are above 25% for both NP1 and NP2, which are significantly higher than those of the aforementioned catalysts.

The recyclability of NP2 was then tested (Figure 4). After each cycle of reaction, the supported catalyst was centrifugated and redispersed in a freshly prepared reaction solution with other compositions identical to the initial run. Such recovery/reinitiation cycles were repeated five times and yielded the oxygen evolution curves 2, 3, 4, 5, and 6. Although the kinetics of oxygen production varied slightly over recycles, the catalyst largely retained O_2 conversion ratio over five recycles, generating 95−86% of the theoretical amount of oxygen gas at 150 min. It can be inferred that there was a minimal

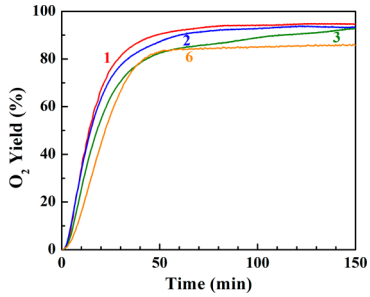

Figure 4. The evolution of oxygen gas catalyzed by NP2 at different cycles. For the numbered cycle *n*, the number *n* indicates the *n*th cycle of the reaction catalyzed by NP2 dispersed in new or renewed solution.

aggregation or leaking of RuO_2, or both the conversion ratio and rate would remarkably deteriorate, as observed in the case of unsupported nanoparticulate RuO_2 catalyzing Ce(IV)-induced water oxidation.[18] Since the catalyst remained quite active after the sixth recycle, the real catalytic capability for conversion should substantially exceed the TON (4 × moles of O_2 produced/mol of RuO_2) of ∼200 calculated from the six runs. In conclusion, the preparation of mesoporous silica-supported RuO_2 nanoparticulates has been optimized to improve the dispersion and size distribution of RuO_2 in the mesoporous framework. Thus obtained NP2 exhibits higher catalytic efficiency than other RuO_2 catalysts in photoinduced water oxidation, and excellent yield, and a quantum efficiency exceeding most metal oxide catalysts in literature. It has the potential to be incorporated into photoinduced water splitting catalytic system as an efficient O_2 evolution cocatalyst.

■ ASSOCIATED CONTENT

Supporting Information

Additional TEM image, small angle XRD patterns, recyclability experimental data, actinometry results, and exemplified and detailed calculation procedures for the data discussed in the main text. This material is available free of charge via the Internet at http://pubs.acs.org.

■ AUTHOR INFORMATION

Corresponding Author

*E-mail: tren@purdue.edu.

Notes

The authors declare no competing financial interest.

■ ACKNOWLEDGMENTS

This research was supported by Purdue University. The authors thank Professor Fabio Ribeiro for the access to instrumentation for the nitrogen sorption experiments. T. Ren acknowledges IR/D support from the U.S. National Science Foundation during the preparation of this manuscript.

■ REFERENCES

(1) Armaroli, N.; Balzani, V. *ChemSusChem* **2011**, *4*, 21−36.
(2) McDaniel, N. D.; Bernhard, S. *Dalton Trans.* **2010**, *39*, 10021−10030.
(3) Sartorel, A.; Carraro, M.; Toma, F. M.; Prato, M.; Bonchio, M. *Energy Environ. Sci.* **2012**, *5*, 5592−5603.
(4) Kiwi, J.; Gratzel, M. *Nature* **1979**, *281*, 657−658.
(5) Hetterscheid, D. G. H.; Reek, J. N. H. *Angew. Chem., Int. Ed.* **2012**, *51*, 9740−9747. Joya, K. S.; Valles-Pardo, J. L.; Joya, Y. F.;

Eisenmayer, T.; Thomas, B.; Buda, F.; de Groot, H. J. M. *ChemPlusChem* **2013**, *78*, 35−47.
(6) Chen, G.; Chen, L. J.; Ng, S. M.; Man, W. L.; Lau, T. C. *Angew. Chem., Int. Ed.* **2013**, *52*, 1789−1791. Grotjahn, D. B.; Brown, D. B.; Martin, J. K.; Marelius, D. C.; Abadjian, M. C.; Tran, H. N.; Kalyuzhny, G.; Vecchio, K. S.; Specht, Z. G.; Cortes-Llamas, S. A.; Miranda-Soto, V.; van Niekerk, C.; Moore, C. E.; Rheingold, A. L. *J. Am. Chem. Soc.* **2011**, *133*, 19024−19027.
(7) Karkas, M. D.; Akermark, T.; Chen, H.; Sun, J. L.; Akermark, B. *Angew. Chem., Int. Ed.* **2013**, *52*, 4189−4193.
(8) Lehn, J. M.; Sauvage, J. P.; Ziessel, R. *Nouv. J. Chim.* **1980**, *4*, 355−358.
(9) Han, H.; Frei, H. *J. Phys. Chem. C* **2008**, *112*, 16156−16159. Junge, H.; Marquet, N.; Kammer, A.; Denurra, S.; Bauer, M.; Wohlrab, S.; Gartner, F.; Pohl, M. M.; Spannenberg, A.; Gladiali, S.; Beller, M. *Chem.—Eur. J.* **2012**, *18*, 12749−12758.
(10) Jiao, F.; Frei, H. *Angew. Chem., Int. Ed.* **2009**, *48*, 1841−1844.
(11) Jiao, F.; Frei, H. *Chem. Commun.* **2010**, *46*, 2920−2922.
(12) Over, H. *Chem. Rev.* **2012**, *112*, 3356−3426.
(13) Kiwi, J.; Gratzel, M. *Angew. Chem., Int. Ed.* **1979**, *18*, 624. Mills, A. *J. Chem. Soc., Dalton Trans.* **1982**, 1213−626. Mills, A. *Chem. Soc. Rev.* **1989**, *18*, 285. Lehn, J.-M.; Sauvage, J.-P.; Ziessel, R. *Nouv. J. Chim* **1979**, *3*, 423−427.
(14) Das, S. K.; Dutta, P. K. *Microporous Mesoporous Mater.* **1998**, *22*, 475−483.
(15) Tuysuz, H.; Schuth, F. *Adv. Catal.* **2012**, *55*, 127−239.
(16) Beck, J. S.; Vartuli, J. C.; Roth, W. J.; Leonowicz, M. E.; Kresge, C. T.; Schmitt, K. D.; Chu, C. T. W.; Olson, D. H.; Sheppard, E. W.; McCullen, S. B.; Higgins, J. B.; Schlenker, J. L. *J. Am. Chem. Soc.* **1992**, *114*, 10834−10843. Kresge, C. T.; Leonowicz, M. E.; Roth, W. J.; Vartuli, J. C.; Beck, J. S. *Nature* **1992**, *359*, 710−712. Vartuli, J. C.; Schmitt, K. D.; Kresge, C. T.; Roth, W. J.; Leonowicz, M. E.; McCullen, S. B.; Hellring, S. D.; Beck, J. S.; Schlenker, J. L.; Olson, D. H.; Sheppard, E. W. *Chem. Mater.* **1994**, *6*, 2317−2326. Beck, J. S.; Vartuli, J. C.; Kennedy, G. J.; Kresge, C. T.; Roth, W. J.; Schramm, S. E. *Chem. Mater.* **1994**, *6*, 1816−1821. Kresge, C. T.; Roth, W. J. *Chem. Soc. Rev.* **2013**, *42*, 3663−3670.
(17) Zhao, D. Y.; Sun, J. Y.; Li, Q. Z.; Stucky, G. D. *Chem. Mater.* **2000**, *12*, 275. Zhao, D.; Feng, J.; Huo, Q.; Melosh, N.; Fredrickson, G. H.; Chmelka, B. F.; Stucky, G. D. *Science* **1998**, *279*, 548−552. Wan, Y.; Zhao, D. Y. *Chem. Rev.* **2007**, *107*, 2821−2860.
(18) Zhang, Y.; Ren, T. *Chem. Commun.* **2012**, *48*, 11005−11007.
(19) King, N. C.; Dickinson, C.; Zhou, W.; Bruce, D. W. *Dalton Trans.* **2005**, 1027−1032.
(20) Chang, K.-H.; Hu, C.-C.; Chou, C.-Y. *Chem. Mater.* **2007**, *19*, 2112−2119.
(21) Yusuf, S.; Jiao, F. *ACS Catal.* **2012**, *2*, 2753−2760.
(22) Ravikovitch, P. I.; Neimark, A. V. *Langmuir* **2002**, *18*, 1550−1560.
(23) Van Der Voort, P.; Ravikovitch, P. I.; De Jong, K. P.; Benjelloun, M.; Van Bavel, E.; Janssen, A. H.; Neimark, A. V.; Weckhuysen, B. M.; Vansant, E. F. *J. Phys. Chem. B* **2002**, *106*, 5873−5877.
(24) Okeyoshi, K.; Yoshida, R. *Adv. Funct. Mater.* **2010**, *20*, 708−714.
(25) Armandi, M.; Hernandez, S.; Vankova, S.; Zanarini, S.; Bonelli, B.; Garrone, E. *ACS Catal.* **2013**, *3*, 1272−1278.
(26) Harriman, A.; Pickering, I. J.; Thomas, J. M.; Christensen, P. A. *J. Chem. Soc., Faraday Trans. 1* **1988**, *84*, 2795−2806.
(27) Yamada, Y.; Yano, K.; Hong, D.; Fukuzumi, S. *Phys. Chem. Chem. Phys.* **2012**, *14*, 5753−5760.
(28) Hong, D.; Yamada, Y.; Nagatomi, T.; Takai, Y.; Fukuzumi, S. *J. Am. Chem. Soc.* **2012**, *134*, 19572−19575.
(29) Morris, N. D.; Mallouk, T. E. *J. Am. Chem. Soc.* **2002**, *124*, 11114−11121.
(30) Hatchard, C. G.; Parker, C. A. *Proc. R. Soc. London, Ser. A* **1956**, *235*, 518−536.
(31) In the reaction suspension, the photosensitizer, catalyst, and silica support all absorb/scatter light, among which only the photosensitizer utilizes the absorbed photons to enable a redox reaction. It was estimated that the ratio between the absorbance of photosensitizer and that of supported catalyst is roughly 4.2:1, which suggests a 24% higher quantum efficiency if the calculation were based only on sensitizer-absorbed photons. However, to obtain a more conservative estimate of the efficiency, the absorption due to the entire suspension was taken into account. Actinometry done indicates that a scattering effect comes into play for long irradiation times, which would lead to a suppression of photon absorbance. This was not accounted for in quantum efficiency calculations and also leads to a more conservative estimate (see Supporting Information Figure S4 for details).
(32) La Ganga, G.; Nastasi, F.; Campagna, S.; Puntoriero, F. *Dalton Trans.* **2009**, *0*, 9997. Puntoriero, F.; La Ganga, G.; Sartorel, A.; Carraro, M.; Scorrano, G.; Bonchio, M.; Campagna, S. *Chem. Commun.* **2010**, *46*, 4725.
(33) Besson, C.; Huang, Z.; Geletii, Y. V.; Lense, S.; Hardcastle, K. I.; Musaev, D. G.; Lian, T.; Proust, A.; Hill, C. L. *Chem. Commun.* **2010**, *46*, 2784.